DESIGN OF A CHEMICAL REACTOR UNDER MICROWAVE IRRADIATION IN RESONANCE CONDITIONS

by

Francesco DESOGUS [*] ***and Renzo CARTA***
Department of Mechanical, Chemical and Material Engineering,
University of Cagliari, Cagliari, Italy

Original scientific paper
https://doi.org/10.2298/TSCI161130173D

Reaction processes often show to be improved by microwave application, but the enhancing effect is not always due solely to the temperature increasing in the medium, which is produced by the radiation exposure. Thus, to study the evolution of such kind of processes needs a strict control of the irradiation conditions and the use of a proper reaction apparatus in which the interaction between radiation and irradiated materials can be precisely defined. The present work is made necessary by the need of operating with controlled and reproducible experimental conditions, and the aim was to design a multi-tube reactor, to work in resonance conditions, inside which the tubes with the fluid to be processed are positioned. In fact, working in resonance conditions allows the irradiated fluid to be exposed to constant microwave power, and the field intensity and power absorption can be accurately calculated and mapped. The cavity was designed by the authors using a proper commercial software for 3-D electromagnetic simulation, then the reactor operation was tested by another commercial multiphysic simulation software. The results here presented show the proper geometrical characteristics of the cavity and of the internal tubes to work at 2.45 GHz of frequency while the irradiation power can be varied depending on the needs of the process. The reactor can work with different homogeneous systems, both chemical and biological (enzyme reactions). The future development will be the construction and the real operation of the designed apparatus in order to confirm the simulation results.

Key words: *chemical reactor, microwave irradiation, resonance conditions, resonant cavity*

Introduction

Microwaves, due to their heating capacity, can enhance chemical processing. Moreover, all chemical and biochemical reactions involve electrical forces between the charged part of the reacting molecules. In fact, chemical binding is a matter of electrical interactions, thought at microscopic scale, thus, an external electromagnetic (EM) field can interact with such reactions [1], and many reports of these interactions were reported in the literature, about both thermal and non-thermal kind [2-7].

However, the application of microwaves in chemical and biochemical processing has not yet been fully exploited, above all in the latter case. The main reason may be the great difficulties of a precise temperature control, which arises in microwave irradiated reactors, and enzymes are very fragile molecules and cannot be subjected to not well controlled reaction

* Corresponding author, e-mail: f.desogus@dimcm.unica.it

conditions. As regards enzyme reactions, improved yields, that cannot be explained just to a thermal effect, have been reported in many cases, like isomerase [8] and amylase [9] catalyzed reactions or lipase catalyzed transesterification (for biodiesel production) [10, 11]. However, the mechanism of the radiation effect on the enzyme activity (and whether it is thermal or non-thermal) is still unclear. A possible explanation could be the action, played by the electric field, of changing the orientation of dipolar molecules and of active sites of the enzyme, which could result in a decrease of the intermolecular distances and in a stricter co-ordination between the reactive groups in substrate molecules and the active sites of the enzyme, thereby leading to enhance the efficiency and the specificity of enzymatic reactions [12, 13]. The effectiveness of non-thermal interactions during chemical, biochemical, and biological processes under microwave irradiation cannot be easily demonstrated, because of the inherent difficulties in conducting such experiments. In fact, non-thermal effects (if they exist) operate concurrently with thermal ones, and it is hard to distinguish between them. However, as it results from most of the studies reported in the literature, microwaves power has not been monitored, or was high enough to give a temperature rise in the medium, so making difficult to quantitatively determine thermal and non-thermal microwave effects. In such studies, even the EM field distribution was not monitored.

Aim of this paper is to design and analyze the behavior of a microwave resonant cavity, to be used as a chemical and biochemical reactor, from the EM point of view. The desired working frequency is 2.45 GHz. Then, the intention is to realize the cavity to be used for evaluating the effect of the EM exposition on the reacting processes. In particular, the attention will be focused on enzyme homogeneous catalyzed reactions performed in a polar (water) medium. As an example simulation case, the enzymatic hydrolysis of sucrose into glucose and fructose will be chosen. The approach here developed and discussed, differently from what presented in the previously cited literature works about enzymatic processes [8-12], allows a precise calculation of the radiation frequency and of the local field in the fluid bulk, which depend both on the shape/dimemsions of the vessel/tubes containing the exposed fluid and on the fluid temperature and dielectric properties.

Materials and methods

Cavity design and simulation

In order to evaluate the effects of the exposition to EM fields in controlled conditions, both for chemical compounds and biological molecules, a suitable exposure apparatus is required, consisting in a resonant cavity in which the reacting mixtures can circulate. To explain the working conditions and the design criteria for this, it is necessary to start from the fundamental equations of electromagnetism, like eqs. (1)-(6), and then to make assumptions and elaborations, with eqs. (7)-(35), to particularize for the conditions here studied. Finally, the EM model will be coupled with the fundamental energy conservation and convection-diffusion equations, see eqs. (36) and (37), in their general form.

Resonant cavities represent a particular case of waveguides, which are devices properly used for confining an EM field inside a spatial region, forcing it to propagate in a fixed direction, conventionally chosen coincident with the axial z-direction. To be more precise, a waveguide is a driving structure with a transverse section which is simply connected and invariant with z (an example may be a metal hollow tube).

The EM field is governed by the Maxwell's equations; in absence of sources, in the phasor domain, for a linear, isotropic, homogeneous and non-dispersive medium, they assume the form:

$$\begin{cases} \nabla \times \mathbf{E} = -j\omega\mu\mathbf{H} \\ \nabla \times \mathbf{H} = j\omega\varepsilon\mathbf{E} \end{cases} \tag{1}$$

in which **E** [Vm^{-1}] and **H** [Am^{-1}] are, respectively, the electric and the magnetic field, ω [s^{-1}] – the angular pulse, ε [Fm^{-1}] and μ [Hm^{-1}] – are, respectively, the electric and the magnetic permittivity, which describe the characteristics of the dielectric material filling the waveguide (air in the present case), and finally j is the imaginary unit.

The transverse and longitudinal (with respect to z) field components can be written:

$$\begin{cases} \mathbf{E} = \mathbf{E}_t + E_z\mathbf{i}_z \\ \mathbf{H} = \mathbf{H}_t + H_z\mathbf{i}_z \end{cases} \tag{2}$$

with

$$\begin{cases} \mathbf{E}_t = E_x\mathbf{i}_x + E_y\mathbf{i}_y \\ \mathbf{H}_t = H_x\mathbf{i}_x + H_y\mathbf{i}_y \end{cases} \tag{3}$$

and

$$\nabla_t = \frac{\partial}{\partial x}\mathbf{i}_x + \frac{\partial}{\partial y}\mathbf{i}_y \tag{4}$$

Now, eq. (1) can be rewritten:

$$\begin{cases} -\dfrac{\partial \mathbf{E}_t}{\partial z} = j\omega\mu\,\mathbf{H}_t \times \mathbf{i}_z - \nabla_t E_z \\ -\dfrac{\partial \mathbf{H}_t}{\partial z} = j\omega\varepsilon\,\mathbf{i}_z \times \mathbf{E}_t - \nabla_t H_z \\ \nabla_t \cdot \left(\mathbf{i}_z \times \mathbf{E}_t\right) = j\omega\mu H_z \\ \nabla_t \cdot \left(\mathbf{H}_t \times \mathbf{i}_z\right) = j\omega\varepsilon E_z \end{cases} \tag{5}$$

From the system eqs. (5), factored solutions must be found, of the kind:

$$\begin{cases} \mathbf{E}_t(x, y, z) = V(z)\mathbf{e}(\mathrm{x}, \mathrm{y}) \\ \mathbf{H}_\mathrm{t}(\mathrm{x}, \mathrm{y}, \mathrm{z}) = I(z)\mathbf{h}(x, y) \end{cases} \tag{6}$$

which represent the system modes, and where $V(z)$ [V] and $I(z)$ [A] are scalar mode functions, while **e** [m^{-1}] and **h** [m^{-1}] are vector mode functions. Substituting the 3rd and 4th of eqs. (5) in the 1st and 2nd equations of the same system, and keeping into account the system of eqs. (6), the following system is obtained:

$$\begin{cases} -\mathbf{e}\dfrac{\mathrm{d}V}{\mathrm{d}z} = j\omega\mu\, I\mathbf{h} \times \mathbf{i}_z - \dfrac{I}{j\omega\varepsilon}\nabla_t\nabla_t \cdot \left(\mathbf{h} \times \mathbf{i}_z\right) \\ -\mathbf{h}\dfrac{\mathrm{d}I}{\mathrm{d}z} = j\omega\varepsilon V\mathbf{i}_z \times \mathbf{e} - \nabla_t\nabla_t \cdot \left(\mathbf{i}_z \times \mathbf{e}\right) \\ V\nabla_t \cdot \left(\mathbf{i}_z \times \mathbf{e}\right) = j\omega\mu H_z \\ I\nabla_t \cdot \left(\mathbf{h} \times \mathbf{i}_z\right) = j\omega\varepsilon E_z \end{cases} \tag{7}$$

where it is notable (from the last two equations) that the factorization of the transverse components implies also the factorization of the longitudinal ones, and consequently of the total field.

To the system of eqs. (7), the boundary conditions must be combined. In the case of ideal waveguides, the walls are made of a perfect electric conductor (PEC), inside of which the electric field is zero. Considering that the continuity conditions for the EM field require the field, tangent to a surface, to be continuous, the boundary condition is:

$$\mathbf{i}_n \times \mathbf{E}\big|_B = 0 \tag{8}$$

in which $\mathbf{i}_n$ is the vector normal to wall and the subscript B indicates the boundary.

To find the solutions of the system of eqs. (7), further conditions are to be assumed on the longitudinal components of field. If $E_z = H_z = 0$ is assumed, both the electric and the magnetic field would result to be transverse to z-direction, thus the modes are transverse electromagnetic (TEM) modes. It can be demonstrated that, for a waveguide with a simply connected transverse section, TEM modes cannot exist.

Other solutions are the modes with only one transverse field, which are the transverse electric (TE, with only $E_z = 0$) and the transverse magnetic (TM, with only $H_z = 0$) modes. If we now consider the latter case (TM, with $H_z = 0$), the system of eqs. (7) becomes:

$$\begin{cases} -\mathbf{e}\dfrac{\mathrm{d}V}{\mathrm{d}z} = j\omega\mu I\mathbf{h}\times\mathbf{i}_z - \dfrac{I}{j\omega\varepsilon}\nabla_t\nabla_t\cdot\left(\mathbf{h}\times\mathbf{i}_z\right) \\ -\mathbf{h}\dfrac{\mathrm{d}I}{\mathrm{d}z} = j\omega\varepsilon V\mathbf{i}_z\times\mathbf{e} \\ V\nabla_t\cdot\left(\mathbf{i}_z\times\mathbf{e}\right) = 0 \\ I\nabla_t\cdot\left(\mathbf{h}\times\mathbf{i}_z\right) = j\omega\varepsilon E_z \end{cases} \tag{9}$$

The second of eqs. (9) can be written:

$$\mathbf{h}(x,y) = \frac{j\omega\varepsilon V(z)}{-\dfrac{\mathrm{d}I(z)}{\mathrm{d}z}}\mathbf{i}_z\times\mathbf{e}(x,y) \tag{10}$$

The left term of eq. (10) depends only on x and y, so also the right term of eq. (10) must depend only on x and y. For this condition being verified, the fraction in the right term must not introduce a dependence on z, so it must be a constant. In this case, eq. (10) can be rewritten:

$$\mathbf{h}(x,y) = A\,\mathbf{i}_z\times\mathbf{e}(x,y) \tag{11}$$

in which A is an arbitrary constant that can be chosen as $A = 1$, thus, the second of eqs. (9) can be rewritten:

$$-\frac{\mathrm{d}I}{\mathrm{d}z} = j\omega\varepsilon V \tag{12}$$

Now, considering eq. (11), the first of eqs. (9) can be adjusted in the form:

$$\nabla_t\nabla_t\cdot\mathbf{e}(x,y) = \frac{j\omega\varepsilon}{I(z)}\left[\frac{\mathrm{d}V(z)}{\mathrm{d}z} + j\omega\mu I(z)\right]\mathbf{e}(x,y) \tag{13}$$

from which, with analogous considerations, it can be deducted that:

$$\nabla_t \nabla_t \cdot \mathbf{e}(x,y) = -K_t^2 \mathbf{e}(x,y) \tag{14}$$

with $-K_t^2$ being constant. Taking into account the last relationship, the first of eqs. (9) can be rewritten:

$$-\frac{\mathrm{d}V}{\mathrm{d}z} = j\omega\mu\left(1-\frac{K_t^2}{\omega^2\varepsilon\mu}\right)I \tag{15}$$

Equations (12) and (15), taken together, form an equation system and are known as *telegrapher's equations*. By introducing the following parameters:

$$\begin{aligned} C &= \varepsilon \\ L &= 1-\frac{K_t^2}{\omega^2\varepsilon\mu} \\ \beta &= \omega\sqrt{LC} = \sqrt{K^2-K_t^2} \\ Z_0 &= \sqrt{\frac{L}{C}} = \frac{K_z}{\omega\varepsilon} \end{aligned} \tag{16}$$

with

$$K = \omega\sqrt{\varepsilon\mu} \tag{17}$$

the solution of the *telegrapher's equations* is:

$$V(z) = V^{\pm}\exp(\mp jK_z z) \tag{18}$$

The single components of eq. (18) represent waves moving along the positive direction of the z-axis in the case of the exponential exp(–$j\beta z$), and along the negative direction of the z-axis in the case of the exponential exp(+$j\beta z$).

The transverse components of the field, that is the vector mode functions, can be obtained by observing that, in eq. (14), **e** is proportional to the transverse gradient of the transverse divergence of **e**, which is the transverse gradient of a scalar function. So, if we put that:

$$\nabla_t \cdot \mathbf{e}(x,y) = K_t \phi(x,y) \tag{19}$$

Equation (14) becomes:

$$\mathbf{e}(x,y) = -\frac{1}{K_t}\nabla_t \phi(x,y) \tag{20}$$

which means that the line integral of **e** on a close curve lying on the transverse plane is zero, and consequently the third of eqs. (9) is verified.

Putting together eqs. (19) and (20), the following relationship can be obtained:

$$\begin{aligned} \nabla_t \cdot \left[-\frac{1}{K_t}\nabla_t \phi(x,y)\right] &= -\frac{1}{K_t}\nabla^2 \phi(x,y) = K_t \phi(x,y) \\ \nabla^2 \phi(x,y) + K_t^2 \phi(x,y) &= 0 \end{aligned} \tag{21}$$

which is the Helmholtz homogeneous equation. To eqs. (21), the boundary condition to respect ϕ must be added. Imposing that the wall tangent field is zero, that is eq. (8), it can be found that ϕ must be zero on the boundary, that is a Dirichlet's condition. Definitely, the problem to be solved becomes:

$$\begin{cases} \nabla^2\phi(x,y) + K_t^2\phi(x,y) = 0 \\ \phi(x,y)\big|_B = 0 \end{cases} \tag{22}$$

In the case of cylindrical waveguides, it is convenient to solve the problem in cylindrical co-ordinates. The system of eqs. (22) is an eigenvalue problem, and could be solved numerically. Probably, the most effective approach is the finite-difference frequency-domain (FDFD) method [14], which can be applied both to scalar [15-21] and to vector [22, 23] problems. As a matter of fact, the FDFD approach, namely the direct discretization of the differential eigenvalue problem, is the simplest numerical strategy to compute eigenvalues and modes of metallic hollow waveguides [23]. The Helmholtz equation, in this co-ordinate system, brings to the Bessel equation, the solution of which is:

$$\phi(\rho,\phi) = J_n(k_t\rho)\left[A\sin(n\phi) + B\cos(n\phi)\right] \tag{23}$$

being $J_n(\psi)$ the Bessel function of the first kind of order n. Imposing the boundary conditions, it can be found that you have the nullification of the ϕ function for the zeroes of the Bessel's function. Indicating with x_{nm} the m^{th} zero of the n order Bessel's function, with a [m] the waveguide radius, and with K [m^{-1}] the wavenumber, the following condition must be verified:

$$K_{t,nm} = \frac{x_{nm}}{a} \tag{24}$$

and the mode can propagate for frequencies higher than its cut-off frequency $f_{c,nm}$:

$$f_{c,nm} = \frac{K_{t,nm}}{2\pi\sqrt{\mu\varepsilon}} = \frac{x_{nm}}{2\pi a\sqrt{\mu\varepsilon}} \tag{25}$$

with the following propagation constant β:

$$\beta = \sqrt{K^2 - K_{t,nm}^2} = \sqrt{K^2 - \left(\frac{x_{nm}}{a}\right)^2} \tag{26}$$

The TE field can be obtained from eq. (20), when expressed in cylindrical co-ordinates:

$$\begin{aligned} E_\rho &= \frac{-jK_z}{K_t}\left[A\sin(n\phi) + B\cos(n\phi)\right]\cdot J_n'(K_t\rho)\cdot \mathrm{e}^{-j\beta z} \\ E_\phi &= \frac{-jK_z n}{K_t^2\rho}\left[A\cos(n\phi) - B\sin(n\phi)\right]\cdot J_n(K_t\rho)\cdot \mathrm{e}^{-j\beta z} \end{aligned} \tag{27}$$

from which it can be noted that the electric field of the TM modes with the index $n = 0$ has a radial direction in all cases.

Once the waveguide modes have been determined, it is possible to obtain the corresponding resonant cavity, considering a waveguide section with a length, d, closed to both the terminal parts with a PEC. In this situation, two waves exist, propagating in both directions

(positive and negative) of z-axis which originate a standing wave. The field can be then expressed in the following form:

$$\mathbf{E}_t = \mathbf{e}(\rho,\phi)\left(E^+ \mathrm{e}^{-j\beta_{nm}z} + E^- \mathrm{e}^{j\beta_{nm}z}\right) \tag{28}$$

The boundary conditions on the new walls closing the waveguide must be the tangent field equal to zero. Assuming that the walls are positioned in $z = 0$ and in $z = d$, from eq. (28) we have that:

$$E^+ = -E^- \tag{29}$$

and

$$E^+ \sin(\beta_{nm} d) = 0 \tag{30}$$

from which

$$\beta_{nm} d = l\pi \quad l = 0,1,2,\ldots \tag{31}$$

Equation (31) requires that the guide length should be an entire number of half wave lengths.

The resonance frequency of the cavity is defined:

$$f_{nml} = \frac{v}{2\pi\sqrt{\varepsilon_r \mu_r}} \sqrt{\left(\frac{x_{nm}}{a}\right)^2 + \left(\frac{l\pi}{d}\right)^2} \tag{32}$$

where v [ms^{-1}] is the speed of light in vacuum, and ε_r and μ_r are the relative electric permittivity and the relative magnetic permeability of the material filling the cavity, respectively. In a resonant cavity, field configurations with frequencies different from the resonance frequencies given by eq. (32) cannot exist.

After defining the geometrical characteristics of the cavity, this has to be fed with an incoming signal. In general terms, the feed is closer to the maximum value of the field of a mode, the bigger is the probability of excite that mode.

An adaptation between the feeding cable and the cavity is necessary to avoid the inlet power being reflected, and so to make it used for the field formation. An important parameter for quantifying the reflected power is the scattering coefficient, Γ, the absolute square value of which allows binding the reflected power to the incident one through the following relationship:

$$P_{\mathrm{ref}} = \left|\Gamma\right|^2 P_{\mathrm{inc}} \tag{33}$$

It is now described the designed apparatus, based on a cylindrical cavity tuned to work at 2.45 GHz (*i. e.*, the frequency allocated for industrial applications) in operating conditions. As a matter of fact, the materials under test are exposed in aqueous solution, so that the cavity must include a suitable container for them. In order to test the effectiveness in chemical processes, it was decided to expose a continuous flow of solution, using a reactor made of eight plexiglass tubes allocated into the cavity, fig. 1. The reactor was centered with respect to the cavity, ensuring a uniform absorption of the EM radiation by the liquid. An external pumping system was to be used, so that the tubes diameter was chosen as to significantly reduce the dispersion of the field outside the cavity. Since the dielectric properties of the fluid under test were essentially the same as those of pure water, the fluid was considered (from the EM point of view) as water, using the Debye model [24] with temperature-dependent parameter [25]. The cavity length was

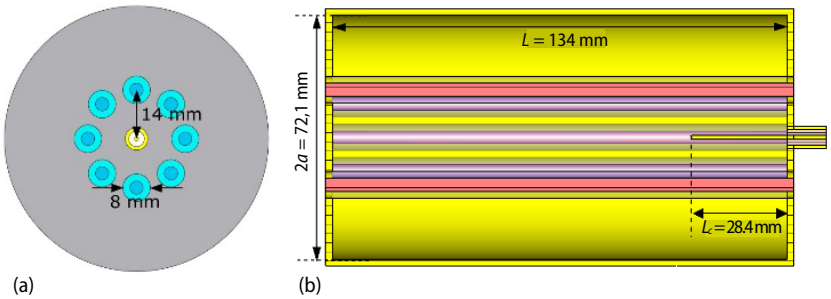

Figure 1. Sketch of the reactor in the resonant cavity; top view (a) and side view (b)

chosen to excite a mode independent from the azimuthal co-ordinate, in order to irradiate in the same way all the tubes. The chosen mode corresponds to the TM_{012} of the empty cavity.

The resonant frequencies of the cavity were obtained by eq. (32) in the form [24]:

$$f_{nml} = \frac{v}{2\pi\sqrt{\varepsilon_{r\_\mathrm{avg}}}}\sqrt{\left(\frac{x_{nm}}{a}\right)^2 + \left(\frac{l\pi}{h}\right)^2} \tag{34}$$

where l, m, n are integers, and x_{nm} are the zeroes of the Bessel's function of the first kind, and $\varepsilon_{r\_\mathrm{avg}}$ is:

$$\varepsilon_{r\_\mathrm{avg}} = \frac{V_\mathrm{a} + V_\mathrm{w}\varepsilon_\mathrm{rw} + V_E\varepsilon_\mathrm{rpl}}{V_\mathrm{a} + V_\mathrm{w} + V_\mathrm{pl}} \tag{35}$$

wherein V_a, V_w, and V_pl are the internal volumes filled with air (a), water (w), and plexiglass (pl), respectively ($V_\mathrm{a}+V_\mathrm{w}+V_\mathrm{pl}=\pi a^2 h$ is the total cavity volume); ε_{rw} and ε_{rp} are the dielectric permittivity of water and plexiglass.

It was chosen for the cavity cylindrical side a commercial size, with a diameter $2a = 72.1$ mm, twice the diameter of a cavity designed in a previous work [26]. Using eq. (34), the height, h, of the cavity, having resonant frequency at 2.45 GHz, is equal to 102.3 mm. However, the previous model did not take into account the inhomogeneous distribution of water (and the spatial variation of the electric field). Actually, a correct approach would be given by eq. (35) with an average weighted by the electric field intensity. Moreover, the imaginary part of the dielectric constant of water cannot be neglected at 2.45 GHz. Therefore, the resonant frequency of the cavity of fig. 1 with $h = 102.3$ mm is different from that given by eq. (34), and equal to 3.046 GHz. Since the application at hand requires a cavity tuned at (or very close to) 2.45 GHz, a tuning of the cavity length, h, was performed. The tuning was done by Compuper Simulation Technology® (CST), in the next section, using the correct (lossy) Debye model for water, with $\tan(\delta) = 0.15$), which gave, for a cavity with the actual structure, the return loss shown in fig. 2, and then the correct height. The final value is $h = 134$ mm, and the Γ behavior of the final cavity is reported in fig. 2.

Of course, the resonant frequency of the designed cavity depends also on the liquid temperature (and increases with it). However, the lossy nature of water allows to feed the cavity also when the liquid is hot. It is clear that the resonant frequency is the required one, with a bandwidth large enough for the applications at hand. However, the electric field distribution is as important as the input match.

Figure 3 shows this distribution at the resonant frequency. It is clear that the field is azimuthally uniform, as required to irradiate all tubes in the same way.

On the other hand, the longitudinal field is not constant but, since the irradiated liquid is flowing, this is not a problem. Actually, the choice of a flow system, instead of a static one, was due to the need of creating well mixing conditions and so of preventing an inhomogeneous microwave exposition. The dimensions of the flow tubes were of the same order of magnitude than the expected thickness of the exposed fluid and the operating conditions made possible to operate in the laminar flow regime. Heat transfer in the fluid was addressed by the following energy conservation equation:

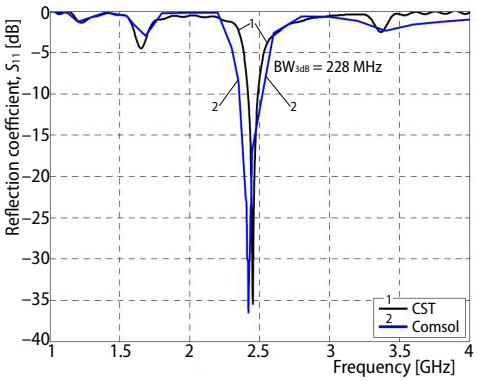

Figure 2. Return loss with probe length L_c = 28.4 mm

$$\rho c_p \mathbf{u} \cdot \nabla T + \nabla\left(-k\nabla T\right) = Q \quad (36)$$

in which **u** [ms^{-1}] is the velocity vector, ρ [kgm^{-3}] represents the fluid density, c_p [Jkg^{-1}K^{-1}] – the heat capacity at constant pressure, T [K] – the temperature, k [Wm^{-1}K^{-1}] – the thermal conductivity, and Q [W] – the thermal power of a generic heat source. Finally, the solute mass transfer (considering the very low concentrations, the approximation of transport of diluted species was adopted) was taken into account by the convection-diffusion equation in the form:

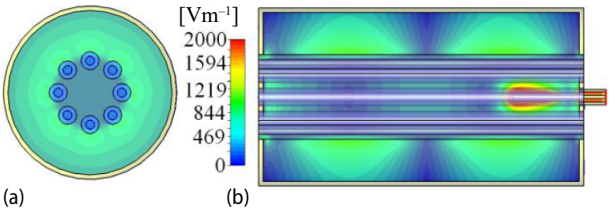

Figure 3. Electric field in the cavity at 2.45 GHz; transverse (a) and longitudinal (b) views (*for color image see journal web site*)

$$\nabla\left(-D_i\nabla M_i\right) + \mathbf{u} \cdot \nabla M_i = R_i \quad (37)$$

in which D_i [m^{2}s^{-1}] is the diffusion coefficient, M_i [molm^{-3}] – the concentration, and R_i [molm^{-3}s^{-1}] – the generation rate for i; the latter was chosen and described by a suitable kinetic model [27, 28].

Design and simulation software

The cavity was designed by the authors using CST Microwave Studio software for 3-D EM simulation. It was drawn with passing-through tubes that do not extend outside the cavity. These pipes were filled with a material which was set up with the dielectric constant and loss tangent of water at the working frequency and at the temperature of 20 °C. A first order Debye's model frequency dependence was used for this material. Moreover, the cavity was surrounded by an air box, on which faces absorption boundary conditions were applied. This allows taking into account the (low) EM field scattered by the opening on the cavity sides.

A more complete simulation would require taking into account the heat transfer and the fluid flowing into the pipes. For this purpose the simulation software COMSOL Multiphysics® was used. An *Electromagnetic Waves, Frequency Domain* analysis, using the same conditions previously stated, showed that the two software packages are in good agreement,

as proven by fig. 2, relative to the reflection coefficient. The fluid dynamics of water was considered using a *Laminar Flow* physic, assuming an average velocity for the incoming fluid on the inlet section. Furthermore, for an enzyme reaction, temperature is a very critical parameter, so a thermal analysis is due and a *Heat Transfer in Fluids* physic was used. This physic allows considering conduction and conduction-convection mechanisms in solids and in the fluid respectively. All these physics were coupled together so that variations of physical parameters affected all the physics.

Results

The multiphysic simulation of section *Cavity design and simulation* was carried out for a possible working microwave power range of 1-300 W and for a fluid average axial velocity range of $5.0 \cdot 10^{-5}$-$1.5 \cdot 10^{-1}$ m/s. The simulation runs gave different, and interesting, results. An example of a simulation output is reported in fig. 4. The main finding was the fact that no significant deviation from the resonance frequency was registered. In fig. 5 the plot of the average temperature in the fluid as a function of the average fluid velocity and of microwave power is reported and the boundary condition is 20 °C for the fluid inlet. It should be highlighted that the temperature is a key parameter in chemical and biochemical kinetic experiments: on one hand, it strongly influences (increases) the process evolution rate and on the other hand, in the case of enzyme reactions, it must be strictly checked and controlled because, if too high, it can irreversibly damage the enzyme molecules. In the case of sucrose hydrolysis catalyzed by invertase enzyme, for example, this limit can be reasonably taken in 60 °C, considering that at this temperature the enzyme loses most of its activity after 60 minutes [29]. From the modeling temperature results it can be pointed out a useful working region for temperatures below 60 °C and velocities in the range $2.0 \cdot 10^{-4}$-$1.5 \cdot 10^{-1}$ m/s for P = 1 W. For increasing power, the available velocity range shrinks (velocity has to be increased and so the process will be carried out with more fluid passages inside the cavity); anyway, the maximum suitable microwave power is 100 W with velocities in the reduced range between $1.0 \cdot 10^{-2}$ and $1.5 \cdot 10^{-1}$ m/s.

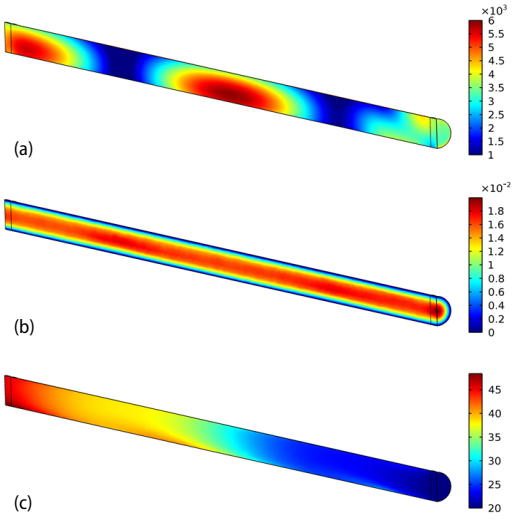

Figure 4. Conditions inside a reaction tube as a result of a multiphysic simulation for a microwave power of 30 W and a fluid average velocity of 0.01 m/s (longitudinal section); (a) electric field distribution, (b) axial component of the fluid velocity, (c) fluid temperature (*for color image see journal web site*)

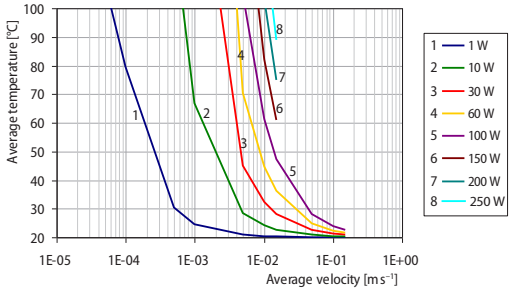

Figure 5. Outlet average temperature of the fluid for different incident microwave powers and average fluid velocities (inlet temperature fixed at 20 °C)

Conclusions

The present study describes the design of a resonant cavity reactor, operating at 2.45 GHz. Thus, the field distribution and the absorption rate were calculated, involving the presence of a flowing fluid characterized by a high value of the dielectric constant, finding out that they are spatially homogeneous in the tube azimuthal direction, so satisfying our planning ideas. However, the longitudinal field distribution presents a much more inhomogeneous distribution, and only several re-circulations of the reacting solution inside the tubes (the fluid motion is in the laminar regime) allow all the fluid elements to be subjected, on average, to the same irradiation conditions throughout the entire treatment.

The possibility to use the resonant cavity reactor here designed as an enzyme reaction apparatus was described and analyzed running multiphysic simulations, with the aim of taking into account the complexity of the interacting phenomena. Besides, the analysis carried out, led to a suitable operating range for microwave power and fluid velocity. In fact, in order to bring (and maintain) the fluid temperature to the value here required for the enzyme reaction, a proper combination of the two parameters, power supply and velocity of the incoming fluid, must be used. So, if a certain electric field intensity is needed, the corresponding power can be supplied and the appropriate velocity can be used to perform the process at the right temperature.

The next steps will be the realization of the experimental reactor prototype, in such a way to carry on real tests and to verify the resonance conditions in real working conditions as well as the simulation results here presented.

References

[1] Buchachenko, A. L., Frankevich, E. L., *Chemical Generation and Reception of Radio- and Microwaves*, VCH Publishers Inc., New York, USA, 1994
[2] Foster, K. R., Thermal and Nonthermal Mechanisms of Interaction of Radio-Frequency Energy with Biological System, *IEEE Transactions on Plasma Science, 28* (2000), 1, pp. 15-23
[3] Carta, R., Desogus, F., The Enhancing Effect of Low Power Microwaves on Phenol Oxidation by the Fenton Process, *Journal of Environmental Chemical Engineering, 1* (2013), 4, pp. 1292-1300
[4] Carta, R., Desogus, F., The Effect of Low-Power Microwaves on the Growth of Bacterial Populations in a Plug Flow Reactor, *AIChE Journal, 56* (2010), 5, pp. 1270-1278
[5] Carta, R., *et al.*, Effect of Microwave Radiation on the Growth Rate of *Bacillus clausii* at 37 °C, *Proceedings*, CHISA – 17th International Congress of Chemical and Process Engineering, Prague, Czech Republic, 2006
[6] Desogus, F., *et al.*, Use of Microwaves for Disinfection of Farmland: A Feasibility Study, *Chemical Engineering Transactions, 52* (2016), Oct., pp. 1195-1200
[7] Spanu, M., *et al.*, Microwaves Disinfection of Farmland, *Journal of Electromagnetic Waves and Applications, 30* (2016), 16, pp. 2165-2173
[8] Yu, D., *et al.*, Microwave Irradiation-Assisted Isomerization of Glucose to Fructose by Immobilized Glucose Isomerase, *Process Biochemistry, 46* (2011), 2, pp. 599-603
[9] Anderson, A. K., Guraya, H. S., Effects of Microwave Heat-Moisture Treatment on Properties of Waxy and Non-Waxy Rice Starches, *Food Chemistry, 97* (2006), 2, pp. 318-323
[10] Molgero Da Ros, P. C., *et al.*, Biodiesel from Babassu Oil: Characterization of the Product Obtained by Enzymatic Route Accelerated by Microwave Irradiation, *Industrial Crops and Products, 52* (2014), Jan., pp. 313-320
[11] Avhad, M. R., Marchetti, J. M., A Review on Recent Advancement in Catalytic Materials for Biodiesel Production, *Renewable and Sustainable Energy Reviews, 50* (2015), Oct., pp. 696-718
[12] Gong, G., *et al.*, Microwave-Assisted Organic Acid Pretreatment for Enzymatic Hydrolysis of Rice Straw, *Biosystems Engineering, 107* (2010), 2, pp. 67-73
[13] Desogus, F., *et al.*, Experimental Study on the Axial Mass Transport of Minced Biomass (Rape Straw) into a Pyrolysis Rotating Reactor Working in the Slipping Regime, *Chemical Engineering Science, 145* (2016), May, pp. 80-89

[14] Fanti, A., Mazzarella, G., Curvilinear Finite Difference Approach to the Computation of Modes of Circular and Elliptic Waveguides, *Proceedings*, IEEE International Conference on Applied Electromagnetics and Communications (ICECom 2010), Dubrovnik, Croatia, 2010
[15] Fanti, A., *et al.*, A Fourth Order FDFD Approach for the Analysis of Sectorial Elliptic Waveguides, *Applied Computational Electromagnetics Society Journal, 30* (2015), 5, pp. 488-495
[16] Fanti, A., *et al.*, Effective Analysis of Ridged Circular Waveguides with a Curvilinear Frequency-Domain Finite-Difference Approach, *Applied Computational Electromagnetics Society Journal, 28* (2013), 11, pp. 1100-1110
[17] Fanti, A., *et al.*, High Order FDFD Computation of all Waveguide Modes Using a Single Grid, *Proceedings*, IEEE Loughborough Antennas and Propagation Conference, Loughborough, UK, 2013
[18] Fanti, A., Mazzarella, G., Finite Difference Single Grid Evaluation of TE and TM Modes in Metallic Waveguides, *Proceedings*, IEEE Loughborough Antennas and Propagation Conference, Loughborough, UK, 2010
[19] Simone, M., *et al.*, Combined PSO-FDFD Optimization of Rectangular Ridged Waveguides, *Applied Computational Electromagnetics Society Journal, 31* (2016), 2, pp. 144-151
[20] Fanti, A., *et al.*, Analysis and Optimization of Elliptic Ridged Waveguide with FDFD Technique and PSO Algorithm, *Applied Computational Electromagnetics Society Journal, 31* (2016), 8, pp. 860-867
[21] Zhao, Y. J., *et al.*, A Compact 2-D Full-Wave Finite-Difference Frequency-Domain Method for General Guided Wave Structures, *IEEE Transactions on Microwave Theory and Techniques, 50* (2002), 7, pp. 1844-1848
[22] Fanti, A., *et al.*, VFD Approach to the Computation TE and TM Modes in Elliptic Waveguide on TM Ggrid, *Applied Computational Electromagnetics Society Journal, 28* (2013), 12, pp. 1205-1212
[23] Fanti, A., *et al.*, Curvilinear Vector Finite Difference Approach to the Computation of Waveguide Modes, *Advanced Electromagnetics, 1* (2012), May, pp. 29-37
[24] Harrington, R. F., *Time-Harmonic Electromagnetic Fields*, McGraw-Hill, New York, USA, 1961
[25] Ray, P. S., Broadband Complex Refractive Indices of Ice and Water, *Applied Optics, 11* (1972), 8, pp. 1836-1844
[26] Maxia, P., *et al.*, A Cylindrical Resonant Cavity to Evaluate the Chemical and Biological Effects of Low-Power RF Electromagnetic Fields, *Microwave and Optical Technology Letters, 54* (2012), 11, pp. 2566-2569
[27] Fanti, A., *et al.*, Evaluation of a Microwave Resonant Cavity as a Reactor for Enzyme Reactions, *Journal of Electromagnetic Waves and Applications, 29* (2015), 17, pp. 2380-2392
[28] Fanti, A., *et al.*, Design and Optimization of a Microwave Irradiated and Resonant Continuous Biochemical Reactor, *Radio Science, 51* (2016), 7, pp. 1199-1212
[29] Vrabel, P., *et al.*, Analysis of Mechanism and Kinetics of Thermal Inactivation of Enzymes: Evaluation of Multitemperature Data Applied to Inactivation of Yeast Invertase, *Enzyme and Microbial Technology, 20* (1997), 5, pp. 348-354

Paper submitted: November 30, 2016
Paper revised: March 31, 2018
Paper accepted: May 13, 2018